Journal of Applied Polymer Science

Epoxy/*p*-phenylenediamine functionalized graphene oxide composites and evaluation of their fracture toughness and tensile properties

Abdelrahman Hussein,[1] Sourav Sarkar,[1] Dongkwon Oh,[2] Kwangju Lee,[2] Byungki Kim[1]

[1]School of Mechatronics Engineering, Korea University of Technology and Education, 1600 Chungjeol-Ro, Byeongcheon-Myeon, Dongnam-Gu, Cheonan Chungnam 31253, Republic of Korea

[2]School of Mechanical Engineering, Korea University of Technology and Education, 1600 Chungjeol-Ro, Byeongcheon-Myeon, Dongnam-Gu, Cheonan Chungnam 31253, Republic of Korea

A.H. and S.S. contributed equally to this article.

Correspondence to: B. Kim (E-mail: byungki.kim@koreatech.ac.kr)

ABSTRACT: In an attempt to enhance the mechanical properties of epoxy/graphene-based composites, the interface was engineered through the functionalization of graphene oxide (GO) sheets with *p*-phenylenediamine; this resulted in *p*-phenylenediamine functionalized graphene oxide (GO–*p*PDA). The morphology and chemical structure of the GO–*p*PDA sheets were studied by spectroscopic methods, thermal analysis, X-ray diffraction, and transmission electron microscopy. The characterization results show the successful covalent functionalization of GO sheets through the formation of amide bonds. In addition, *p*-phenylenediamine were polymerized on graphene sheets to form crystalline nanospheres; this resulted in a GO/poly(*p*-phenylenediamine) hybrid. The mechanical properties of the epoxy/GO–*p*PDA composite were assessed. Although the Young's modulus showed improvement, more significant improvements were observed in the strength, fracture strain, and plane-strain fracture toughness. These improvements were attributed to the unique microstructure and strong interface between GO–*p*PDA and the epoxy matrix. © 2016 Wiley Periodicals, Inc. J. Appl. Polym. Sci. **2016**, *133*, 43821.

KEYWORDS: composites; functionalization of polymers; graphene and fullerenes; mechanical properties; nanotubes

Received 3 February 2016; accepted 24 April 2016

DOI: 10.1002/app.43821

INTRODUCTION

Polymer nanocomposites have gained tremendous academic and industrial interest since their discovery 2 decades ago.[1] Their main advantage is that they show remarkable improvements in properties at very low nanofiller contents and thus do not affect the density and liquid viscosity.[2–4] Among various nanofillers, graphene is one of the most actively studied nanofillers for different types of polymers, including poly(methyl methacrylate),[5] epoxy,[6] polyamide,[7] and elastomers.[8] This is due to its exceptional mechanical, thermal, and electrical properties.[9–12] Despite its organic nature, the engineering of the interface between graphene and the polymer matrix plays an important role in the realization of the full potential of graphene for property improvement, although graphene's exceptional mechanical properties, its two-dimensional large surface area, and van der Waal's interaction result in sheet agglomeration.[13] In addition, from a structural point of view, although pristine graphene had a remarkable stiffening effect, its other mechanical properties did not show tangible improvements because of its poor interfacial properties.[14] One effective method for solving this problem is the introduction of functional groups that can link graphene sheets and the polymer matrix.[15]

For the epoxy matrix, the attachment of amine-terminated functionalities to graphene is the most suitable because they can attach to the epoxy monomer through an epoxide ring-opening reaction.[3] Different amines have successfully functionalized graphene; these include ethylenediamine[16] and hexamethylene diamine.[17] Aromatic amines, such as *p*-phenylenediamine (*p*PDA), were attached to graphene and applied to supercapacitors,[18] dopamine detection,[19] and gas sensors.[20] *p*PDA is expected to prevent graphene sheets from agglomeration because of its bulky aromatic structure. In addition, the presence of a primary amine bifunctionality allows for attachment with graphene from both sides: one side through the amidation of carboxylic groups on graphene oxide (GO)[21] and the other side through a ring-opening reaction with epoxy monomer (Figure 1). It has also been reported that *p*PDA simultaneously reduces GO while attaching with a reduction efficiency that is comparable to hydrazine.[22]

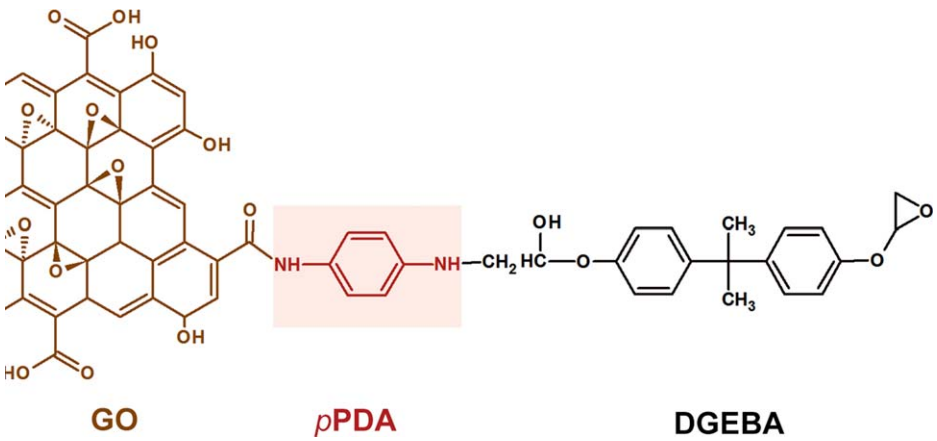

Figure 1. Proposed chemical linkage of GO with epoxy through the bifunctionality of *p*PDA. [Color figure can be viewed in the online issue, which is available at wileyonlinelibrary.com.]

The study of the mechanical properties of epoxy reinforced with GO–*p*PDA has not been covered well in the literature. In this article, we report the synthesis of GO–*p*PDA via a thermal annealing method in an aqueous medium. Physical and chemical characterizations are also reported. Epoxy/GO–*p*PDA composites were fabricated via a solution mixing process. Mechanical reinforcement in terms of the tensile and fracture toughness (K_{Ic}) properties are presented.

EXPERIMENTAL

Materials

Graphite (45 μm flake size, grade 230U) was kindly provided by Asbury Carbons. Fuming HNO_3 (>90%) and $KClO_3$ (98%) were purchased from Sigma-Aldrich. H_2SO_4 (95–98%), HCl (37%), and *p*PDA (97%) were obtained from Alfa-Aesar. Epoxy resin [diglycidyl ether of bisphenol A (DGEBA); Epon 828] was obtained from Hexion. Diethylenetriamine hardener was obtained from New Seoul Chemical Co., Ltd.

Synthesis of GO

GO was prepared by the Staudenmaier method.[23] Graphite flakes (5 g) were added to an acid mixture: 45 mL of HNO_3 to 87.5 mL of H_2SO_4 in a beaker with vigorous stirring with a magnetic stirrer. An amount of 55 g of the oxidizing agent ($KClO_3$) was added gradually during the 4 days of reaction. The graphite oxide slurry was then washed thoroughly with a 5% HCl solution and then in purified water several times. The slurry was vacuum-filtered and then dried in a vacuum oven for 24 h at 60 °C.

Functionalization of GO with *p*PDA

An amount (100 mg) of GO were ultrasonicated in a 100 mL aqueous solution until a brown homogeneous solution was formed. Meanwhile, 500 mg of *p*PDA was dissolved in a 200 mL aqueous solution at 70 °C for 1 h until a homogeneous dark red solution was obtained. The GO dispersion was added to the *p*PDA solution and ultrasonicated for 60 min; it was then stirred with a magnetic stirrer for 48 h at 70 °C. The mixture was allowed to cool down and then thoroughly washed to remove excess *p*PDA. The precipitated slurry was vacuum-filtered and dried in a vacuum oven at 60 °C.

Composite Fabrication

Composite specimens were fabricated by a solution-mixing method, in which calculated amounts of GO–*p*PDA were dispersed in 10 mL of *N*,*N*-dimethylformamide with ultrasound for 30 min. The dispersion was then mixed with epoxy resin with a mechanical stirrer at 1000 rpm for 30 min at 50 °C and then with ultrasound for another 60 min. The mixture was then degassed in a vacuum oven for 1 h and left to cool down to room temperature. Diethylenetriamine hardener was then added (stoichiometric ratio = 12 pph) and mixed in a shear mixer (Kakuhunter SK-300S, Shashin Kagaku) at 2000 rpm for 1 min to prevent excessive heating and premature curing. The mixture was poured in silicone molds, cured at 45 °C for 60 min, and then postcured at 100 °C for 2 h.

Characterization and Instruments

Chemical functionalization with *p*PDA was measured by Fourier transform infrared (FTIR) spectroscopy (Bruker, Hyperion 3000), and X-ray photoelectron spectroscopy (XPS; Thermo Scientific, k-Alpha). Thermal analysis was performed with differential scanning calorimetry (DSC; PerkinElmer, DSC4000) and thermogravimetric analysis (TGA; TA Instruments, TGAQ500). Microstructural studies were performed with X-ray diffraction (XRD; PANalytical, Empyrean), scanning electron microscopy (SEM; FEI, Helios600i), and transmission electron microscopy (TEM; FEI, Tecnai F30 S-Twin). Tensile testing was performed according to ASTM D 638-02a with a tensile testing machine (MTS 810 materials testing system) at a crosshead speed of 1 mm/min. Type-II geometry was used with a gage length of 50 mm, a width of 6 mm, and a thickness of 4 mm. Mode I K_{Ic} was measured according to ASTM D 5045-99 for compact-tension configuration. Natural cracking was created by the tapping of a fresh razor blade. This process generated instantly propagated cracks with lengths of up to several millimeters. However, to retain the standard recommendations, only natural cracks with lengths of 0.5–0.8 mm are reported. Natural crack lengths were measured after fracture testing. The K_{Ic} values were determined according to the relationships:

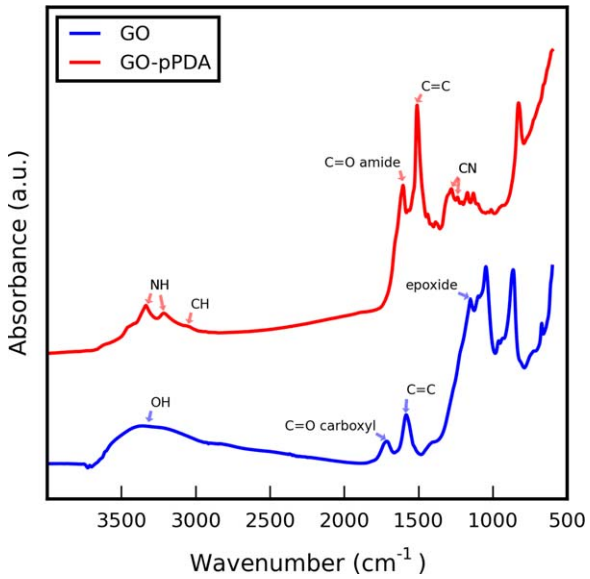

Figure 2. FTIR spectra of GO and GO–*p*PDA. The main functional groups are indicated. [Color figure can be viewed in the online issue, which is available at wileyonlinelibrary.com.]

$$K_Q = \frac{P_Q}{BW^{1/2}} f(x) \tag{1}$$

$$f(x) = \frac{(2+x)(0.886+4.64x-13.32x^2+14.72x^3-5.6x^4)}{(1-x)^{3/2}} \tag{2}$$

$$x = a/W \tag{3}$$

where P_Q is the peak load (kN), $f(x)$ is a CT (compact tension) geometry dependent factor, K_Q is the conditional fracture toughness (MPa $m^{1/2}$), B is the specimen thickness (1 cm), W is

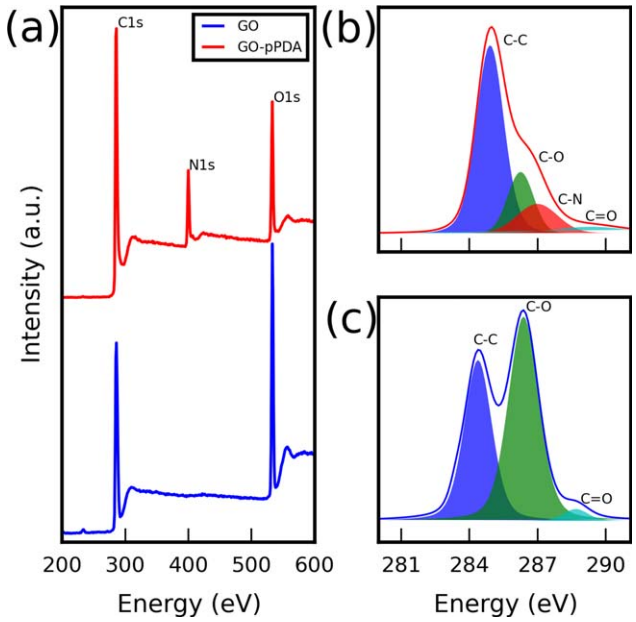

Figure 3. (a) XPS spectra of GO and GO–*p*PDA and (b,c) C1s spectra of GO–*p*PDA and GO, respectively. [Color figure can be viewed in the online issue, which is available at wileyonlinelibrary.com.]

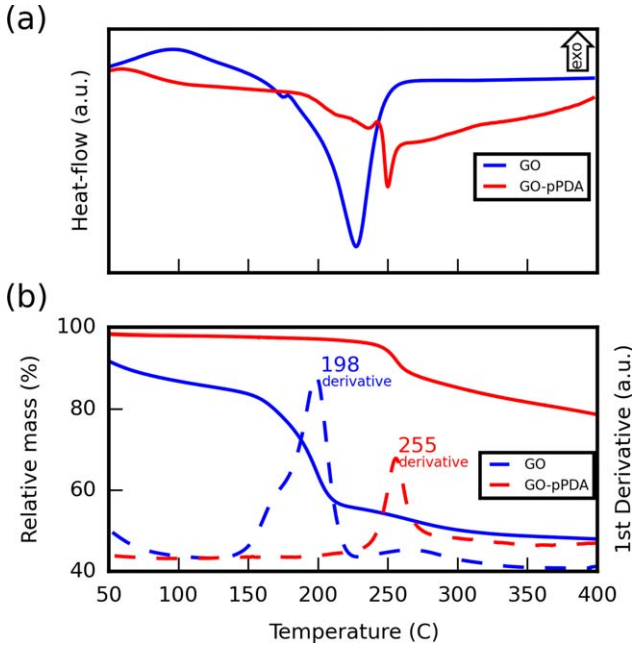

Figure 4. Thermal analyses of GO and GO–*p*PDA: (a) DSC and (b) TGA. [Color figure can be viewed in the online issue, which is available at wileyonlinelibrary.com.]

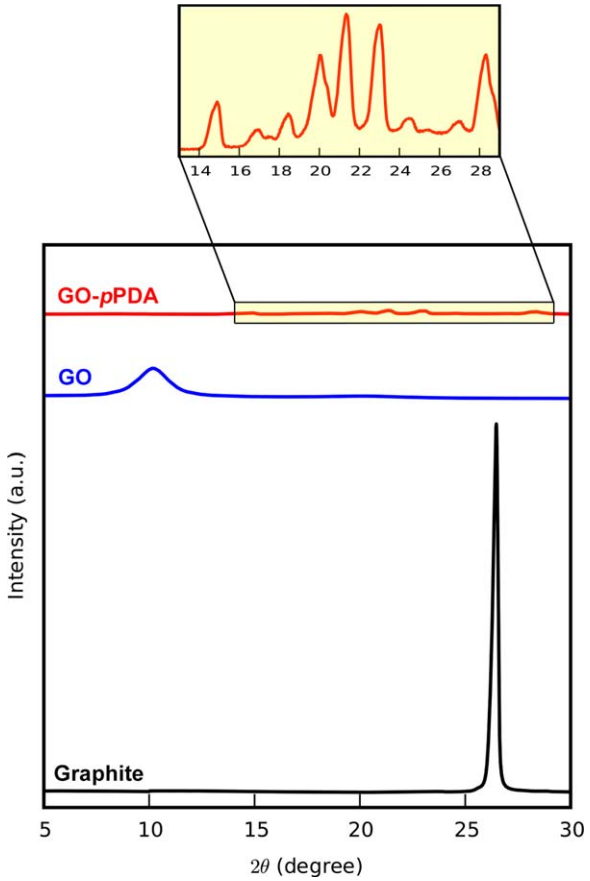

Figure 5. XRD spectra of graphite, GO, and GO–*p*PDA. In the inset, the *y*-axis magnification shows the relatively weak peaks of GO–*p*PDA. [Color figure can be viewed in the online issue, which is available at wileyonlinelibrary.com.]

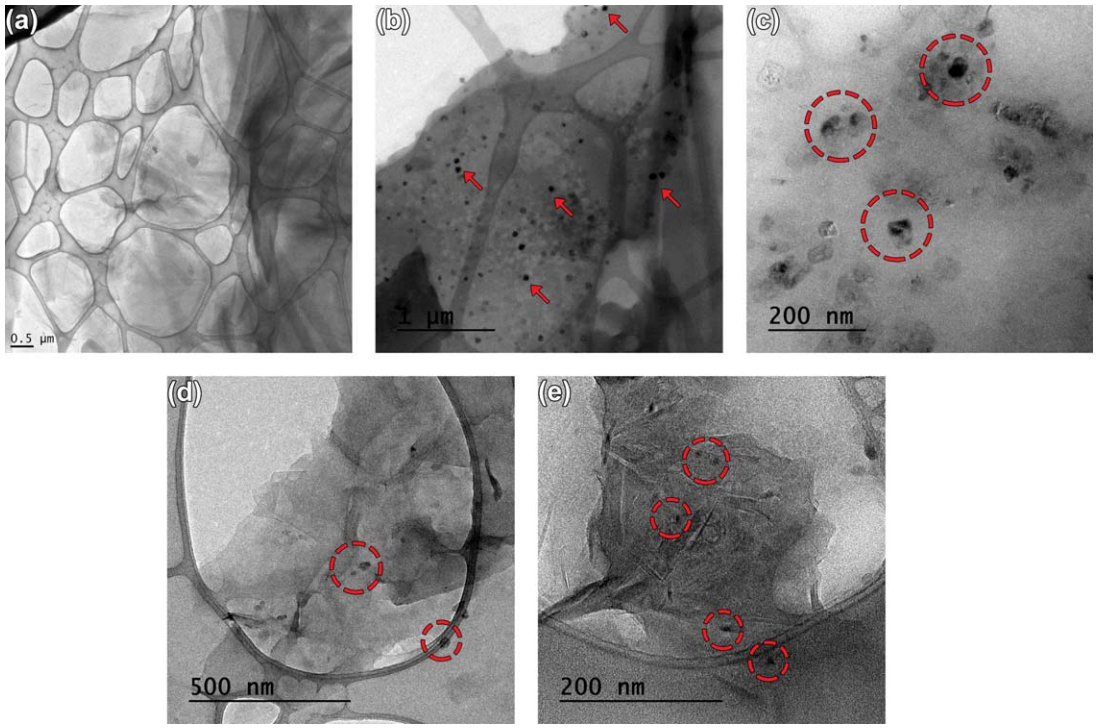

Figure 6. TEM images of (a) GO, (b,c) GO–*p*PDA dispersed in water, and (d,e) GO–*p*PDA dispersed in NMP. The red circles and arrows point to the polymeric *p*PDA crystallites formed on the GO surface. [Color figure can be viewed in the online issue, which is available at wileyonlinelibrary.com.]

the specimen width (10 cm), and *a* is the crack length (1.05–1.08 cm). For both mechanical tests, an average of at least four samples is reported.

RESULTS AND DISCUSSION

Characterization Results

The functionalization of GO with *p*PDA was studied with spectroscopic and thermal analysis methods. FTIR analysis (Figure 2) shows the presence of different functional groups in GO. The —OH group was identified by the broad peak around 3300 cm^{-1}. Carboxyl and carbonyl groups were identified by peaks at 1717 and 1588 cm^{-1}, respectively. The peak at 1155 cm^{-1} corresponded to the epoxide group. The FTIR spectrum of the GO–*p*PDA sample showed a partial reduction of the functional groups of GO and the appearance of new functional groups. The intensity of the broad —OH peak decreased with the superposition of two peaks at 3325 and 3125 cm^{-1}; this corresponded to —NH stretching.[24] The carboxyl peak at 1717 cm^{-1} shifted to 1606 cm^{-1}, and this peak was assigned to carbonyl amide (C═O) stretching.[25] This indicated that *p*PDA was covalently attached to GO via amide bonds through carboxylic acid.[21] The carbonyl peak shifted to 1480 cm^{-1}. C—N was identified by a double peak at 1279 and 1238 cm^{-1}.[19]

More quantitative information with respect to the chemical composition and functional groups were extracted from XPS analysis. Figure 3(a) shows the XPS spectra of GO and GO–*p*PDA. GO showed two dominant peaks at 286.08 and 533 eV, which corresponded to the C1s and O1s bands, respectively. The GO–*p*PDA spectra showed the same peaks in addition to a third peak at 400.08 eV; these corresponded to the N1s band. XPS analysis further confirmed the simultaneous reduction and covalent functionalization of GO. First, quantitative elemental analysis showed the reduction of the C/O ratio from 2.42 to 5.33 for GO–*p*PDA. The high-resolution analysis shown in Figure 3(b,c) showed the reduction of the C—O bond in GO–*p*PDA along with the emergence of a C—N peak.

Thermal analysis provided information about the thermal stability due to the chemical structure. As shown in Figure 4(a), the DSC scans showed an endothermic peak around 220 °C; these indicated the thermal decomposition of the oxygenated functional groups. GO–*p*PDA had an endothermic peak at a temperature of 250 °C. Furthermore, TGA in Figure 4(b) showed a steep mass loss at 198 °C with about a 50% mass loss at 400 °C. GO–*p*PDA showed a less steep mass loss at about 255 °C with a total mass loss of about 20% at 400 °C. The chemical and thermal analysis results suggest the successful covalent functionalization of *p*PDA with GO to form a more thermally stable GO–*p*PDA.

Microstructural identification with XRD is shown in Figure 5. The peak at a 2θ of about 26.5 ° in graphite showed that the interplanar spacing of the graphitic planes was 0.337 nm. For GO, this peaks shifted to about 10.18 °; this indicated an increase in the spacing of graphitic planes to 0.864 nm due to oxidation. For GO–*p*PDA, the relatively low intensity peaks are shown more clearly in the Figure 5 inset. The graphitic peaks vanished; this indicated the full exfoliation of the graphitic planes and the formation of new multiple peaks. This indicated the formation of a new crystalline phase. Partially crystalline poly(*p*-phenylenediamine) (poly-*p*PDA) microparticles showed a relatively similar XRD pattern.[24,26] This suggested that the *p*PDA formed small polymeric crystallites on the GO sheets.

The TEM micrographs in Figure 6 support the claim of formation of polymeric crystallites on GO. Compared to the plain GO surface [Figure 6(a)], GO–*p*PDA [Figure 6(b,c)] had dark dots. We believe this was the crystalline phase in XRD. Liu *et al.*[19] polymerized GO on the surface of GO with a similar procedure. Poly-*p*PDA could be fabricated by a simple annealing procedure[19] in an aqueous medium in the presence of an oxidizing medium. Jaidev and Ramaprabhu[27] observed a similar morphology for hydrogen-reduced GO with high-resolution TEM during the *in situ* chemical oxidative polymerization of excess *p*PDA in the presence of $K_2S_2O_8$ as an oxidizing agent.

Because of the lack of chemical probing on such a small scale, we performed a simple experiment to validate our claim. *p*PDA is soluble in aqueous media, whereas poly-*p*PDA is soluble in *N*-methyl-2-pyrrolidone (NMP).[28,29] Two samples of GO–*p*PDA were sonicated, one in NMP and the other in water. The NMP sample turned the solution turned dark red as an indication of the dissolution of poly-*p*PDA on the GO surface, whereas the aqueous solution turned faint pink as an indication of the slight solubility of poly-*p*PDA in an aqueous medium. The TEM micrographs of the samples in Figure 6(d,e) indeed showed that the dark dots became fainter.

Proposed Reaction Mechanism

On the basis of the characterization results, the reaction mechanism illustrated in Figure 7 is proposed. With the addition of GO to *p*PDA, there was a π–π stacking interaction between GO and *p*PDA.[30] A redox reaction was responsible for the covalent functionalization of *p*PDA with GO[19] through amide-bond formation. The carboxylic group in GO was reduced, and one of the two primary amine groups in the *p*PDA molecule was oxidized.[21,31] Then, GO acted as the oxidizing agent for the oxidative polymerization process. The chemical oxidative polymerization of *p*PDA in acidic medium resulted in fine, uniform polymer particles.[24] Thus, because of the acidic nature of GO,[32] the poly-*p*PDA nanocrystallites had a uniform spherical morphology.

Mechanical Properties

The results of tensile testing are shown in Figure 8. The addition of GO–*p*PDA significantly enhanced the mechanical properties of the composite. The Young's modulus showed a relatively slight enhancement [Figure 8(b)] with an increase from 1.45 GPa for the neat epoxy to 1.52 GPa for the 0.05% GO–*p*PDA loading. A further increase in the GO–*p*PDA loading reduced back to become almost equal or less than the neat epoxy value. The lowest Young's modulus was for the 0.5% loading. Although GO–*p*PDA was thought to have a better interface with the epoxy matrix, there were two possible reasons for that behavior. First, the high-quality, single-sheet graphene had a Young's modulus of 1 TPa,[12] whereas GO had a lower modulus of about 200 GPa.[33] Additionally, the poly-*p*PDA nanospheres on the GO sheets were thought to have a significantly lower Young's modulus; this further reduced the stiffening effect of GO. In that sense, this behavior resembled the effect of the three-phase rubber-modified epoxy nanocomposites.[34,35] The hard phase, silica or clay particles, together with the soft phase had a balanced effect on toughening without excessively reducing the modulus.

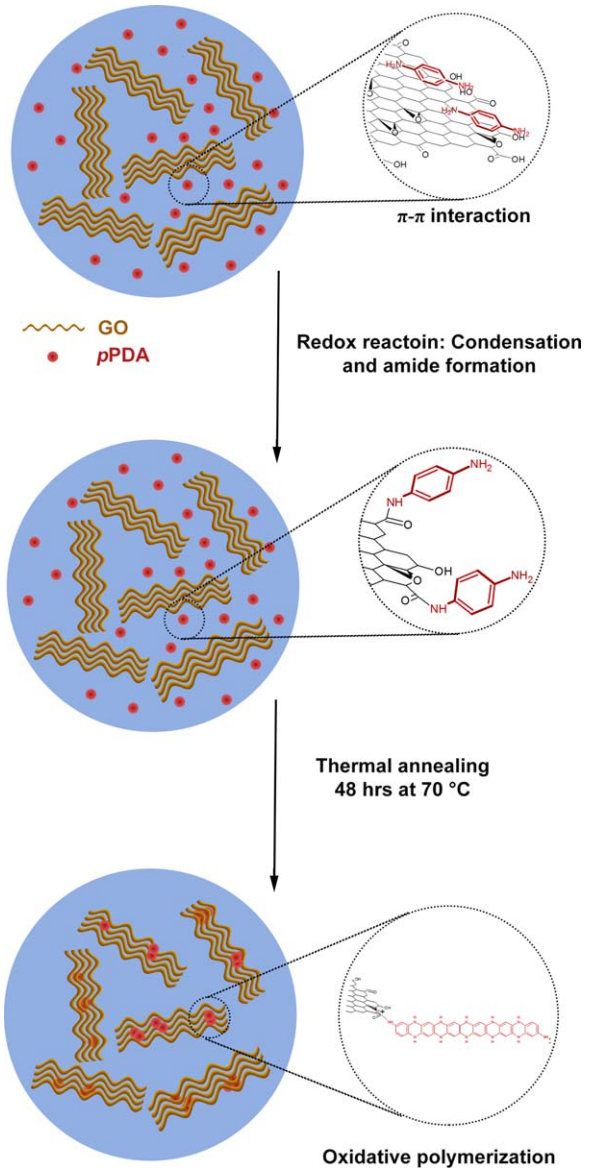

Figure 7. Schematic illustration of the proposed reaction mechanism between GO and *p*PDA. [Color figure can be viewed in the online issue, which is available at wileyonlinelibrary.com.]

GO–*p*PDA had a more profound effect on the tensile strength, interestingly, simultaneously with the fracture strain [Figure 8(c,d)]. The 0.05% GO–*p*PDA increased the strength to 68.6 MPa; this was an almost 25% increase compared to that of the neat epoxy along with a strain at break of about 11.1%. The strength fluctuated with a further increase in GO–*p*PDA up to 0.5%; however, it was almost in the same range. The strain at break showed a similar trend in the same range of GO–*p*PDA contents with a minimal break strain of 7.96%; this was still higher than that of the neat epoxy, which had a strain at break of 6.37%. Above 0.5%, there was a significant deterioration in the properties until a minimum was reached at 2% GO–*p*PDA. The improvement in strength was attributed to the enhanced interface with the epoxy matrix due to functionalization; this was confirmed by the fractography studies,[13,25] as shown in Figure 9. Neat epoxy had a clean fracture surface as an indication of brittle

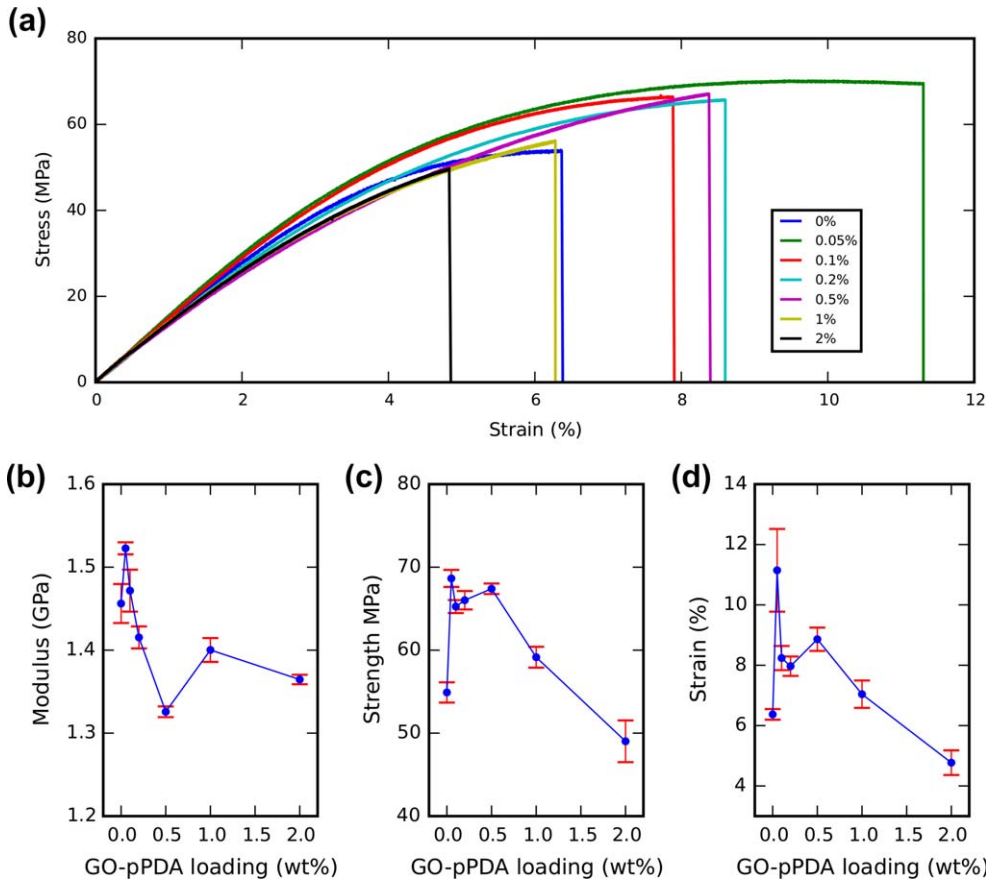

Figure 8. (a) Representative stress–strain curves, (b) Young's modulus, (c) tensile strength, and (d) strain at break of the composites at different loadings of GO–*p*PDA. [Color figure can be viewed in the online issue, which is available at wileyonlinelibrary.com.]

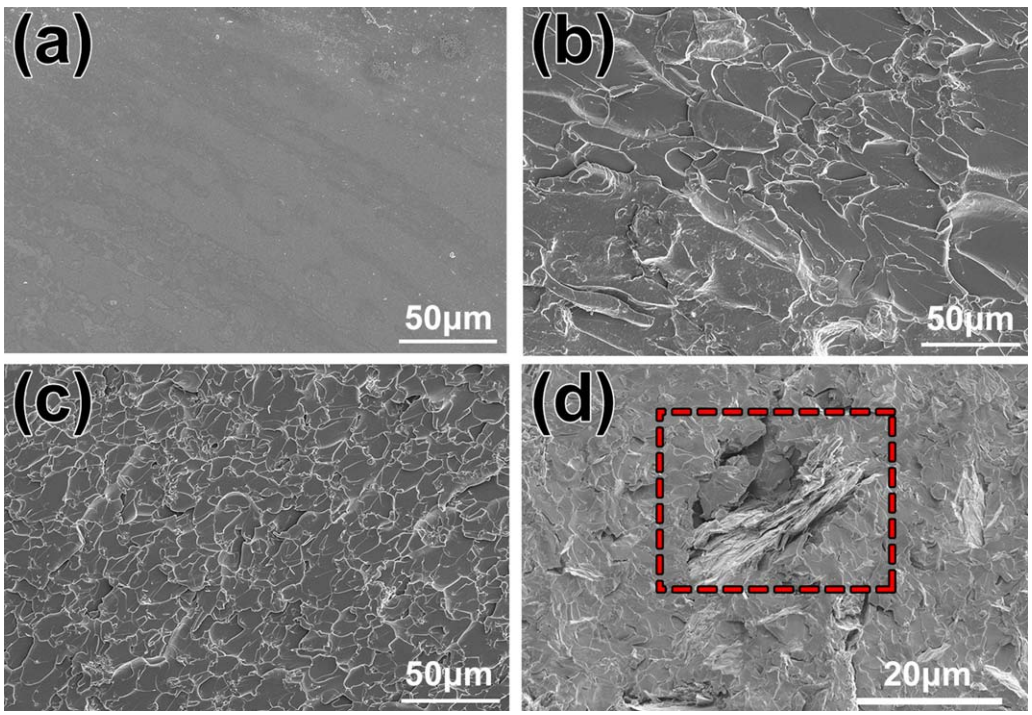

Figure 9. SEM micrographs of the fractured surfaces after tensile testing of the selected samples: (a) neat epoxy, (b) 0.05% GO–*p*PDA, (c) 0.5% GO–*p*PDA, and (d) 2% GO–*p*PDA. The square indicates an agglomeration of GO–*p*PDA. [Color figure can be viewed in the online issue, which is available at wileyonlinelibrary.com.]

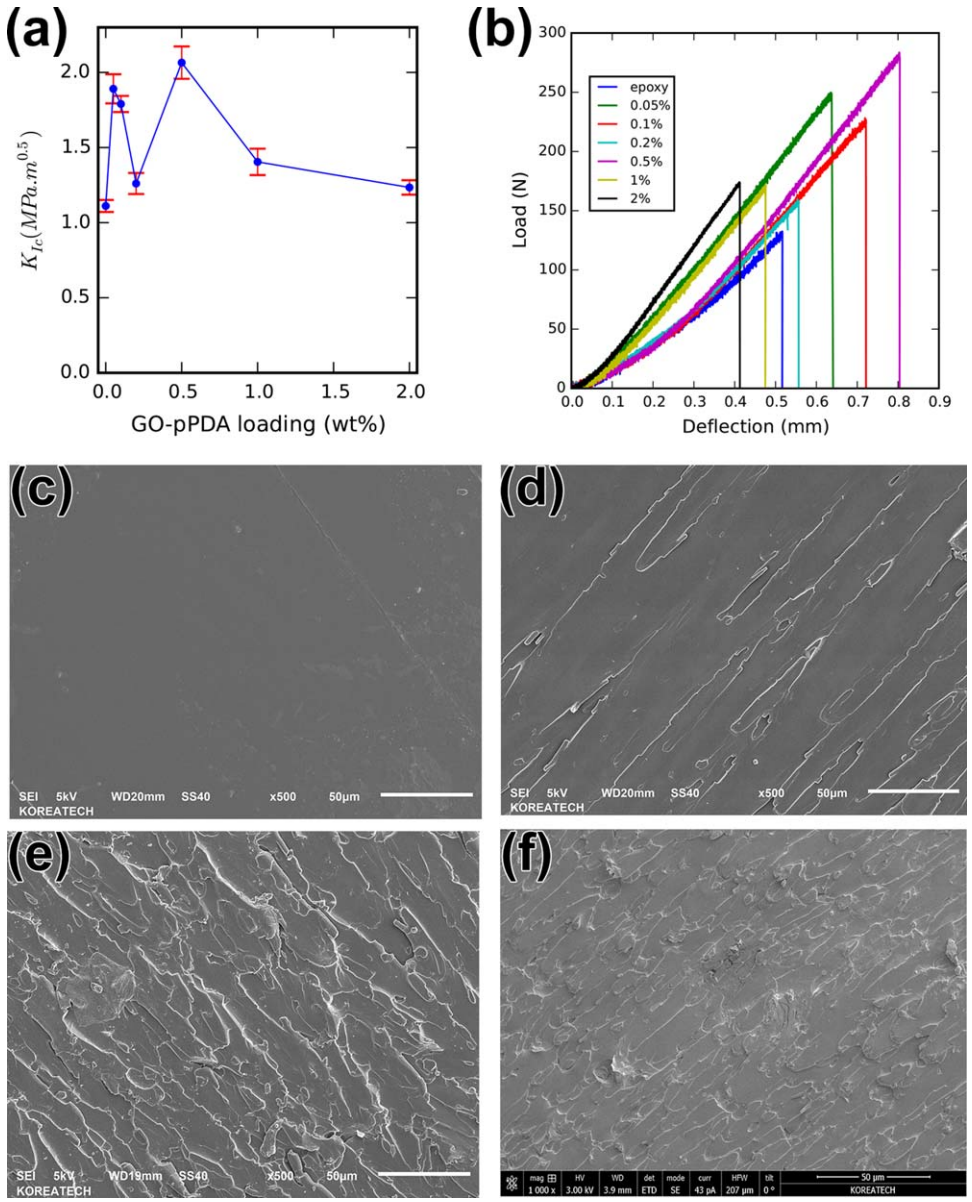

Figure 10. (a) K_{Ic} results at different loadings, (b) load–deflection curves of the tests, and (c–f) fractured surface micrographs at GO–*p*PDA loadings: 0, 0.05, 0.5, and 2%, respectively. [Color figure can be viewed in the online issue, which is available at wileyonlinelibrary.com.]

fracture. The GO–*p*PDA composites (0.05 and 0.5%) had a rough surface as an indication of ductile fracture and more resistance to microcrack propagation. The 2% composite showed highly agglomerated particles; this was responsible for the poor properties. The simultaneous enhancement of the breaking strain could be explained by the toughening effect from the K_{Ic} studies.

The plane-strain K_{Ic} results are shown in Figure 10(a). The representative load–deflection curves of the fracture tests are shown in Figure 10(b). The 0.05% GO–*p*PDA had a significant K_{Ic} of 1.89 MPa $m^{0.5}$ compared to the neat epoxy with a K_{Ic} of 1.11 MPa $m^{0.5}$. This value was close to the K_{Ic} value obtained by Wang *et al.*[36] for the submicrometer GO–epoxy system at a 0.05% loading. The 0.1 and 0.2% GO–*p*PDAs showed drops in K_{Ic} above that of the neat epoxy. The 0.5% loading showed the maximum K_{Ic} of 2.06 MPa $m^{0.5}$. It is worth noting that 0.5% GO–*p*PDA, with the maximum toughening effect, showed the lowest Young's modulus; this showed the role of the *p*PDA polymer phase. A further increase in GO–*p*PDA to 1 and 2% reduced K_{Ic} to almost the value of the neat epoxy. The toughening effect of GO–*p*PDA was attributed to the synergistic crack deflection mechanism that characterizes two-dimensional materials,[36] a strong interface with the matrix,[37] and the presence soft *p*PDA nanoparticles.[33,34] Again, this was confirmed by the fractography studies. Figure 10(c–f) shows SEM of the K_{Ic} fractured surfaces of the composite at representative GO–*p*PDA contents. Neat epoxy showed a typical brittle fractured surface without any resistance to crack propagation. On the other hand, the GO–*p*PDA/epoxy composites showed a rough flaky surface with increasing roughness with increasing GO–*p*PDA content. This indicated that the resistance of crack propagation

by crack deflection around the GO–*p*PDA flakes. Additionally, the flaky surface indicated the strong interface between GO–*p*PDA and the epoxy matrix. This resulted in a greater crack energy absorbance compared to that of neat epoxy matrix; thus, the composites effectively resisted crack propagation.

CONCLUSIONS

In this study, GO functionalized with *p*PDA was successfully synthesized via a thermal annealing process in an aqueous medium. Chemical and thermal characterizations confirmed covalent functionalization. Microstructural characterization via TEM and XRD showed the formation of crystalline nanoparticles on GO; these were explained to be poly-*p*PDA formed via oxidative polymerization. This led to the formation of the GO–poly-*p*PDA hybrid. However, additional study is required for the identification of this new polymeric phase. The application of this unique hybrid as a reinforcement to epoxy resin enhanced the fracture strength and strain with a small effect on Young's modulus. Additionally, a remarkable toughening effect was observed. The main reason for this was the unique GO–*p*PDA structure, which worked as a two-phase filler with an enhanced interface with the epoxy matrix.

ACKNOWLEDGMENTS

This work was generously supported by the Space Core Technology Program through the National Research Foundation of Korea, which was funded by the Ministry of Science, Information and Communications Technology, and Future Planning (contract grant number 2013M1A3A3A02042257). This work is also partially supported from KOREATECH 2013 Research Grant for New Professors.

REFERENCES

1. Usuki, A.; Kojima, Y.; Kawasumi, M.; Okada, A.; Fukushima, Y.; Kurauchi, T.; Kamigaito, O. *J. Mater. Res.* **1993**, *8*, 1179.
2. Paul, D. R.; Robeson, L. M. *Polymer* **2008**, *49*, 3187.
3. Azeez, A. A.; Rhee, K. Y.; Park, S. J.; Hui, D. *Compos. B* **2013**, *45*, 308.
4. Safarabadi, M.; Mehri Khansari, N.; Rezaei, A. *Eng. Solid Mech.* **2014**, *2*, 173.
5. Ramanathan, T.; Abdala, A. A.; Stankovich, S.; Dikin, D. A.; Herrera-Alonso, M.; Piner, R. D.; Adamson, D. H.; Schniepp, H. C.; Chen, X.; Ruoff, R. S.; Nguyen, S.; Aksay, I. A.; Prud'homme, R. K.; Brinson, L. C. *Nat. Nanotechnol.* **2008**, *3*, 327.
6. Rafiee, M. A.; Rafiee, J.; Wang, Z.; Song, H.; Yu, Z.-Z.; Koratkar, N. *ACS Nano* **2009**, *3*, 3884.
7. O'Neill, A.; Bakirtzis, D.; Dixon, D. *Eur. Polym. J.* **2014**, *59*, 353.
8. Frasca, D.; Schulze, D.; Wachtendorf, V.; Huth, C.; Schartel, B. *Eur. Polym. J.* **2015**, *71*, 99.
9. Geim, A. K.; Novoselov, K. S. *Nat. Mater.* **2007**, *6*, 183.
10. Balandin, A. A.; Ghosh, S.; Bao, W.; Calizo, I.; Teweldebrhan, D.; Miao, F.; Lau, C. N. *Nano Lett.* **2008**, *8*, 902.
11. Kim, K. S.; Zhao, Y.; Jang, H.; Lee, S. Y.; Kim, J. M.; Kim, K. S.; Ahn, J.-H.; Kim, P.; Choi, J.-Y.; Hong, B. H. *Nature* **2009**, *457*, 706.
12. Lee, C.; Wei, X.; Kysar, J. W.; Hone, J. *Science* **2008**, *321*, 385.
13. Shen, B.; Zhai, W.; Tao, M.; Lu, D.; Zheng, W. *Compos. Sci. Technol.* **2013**, *77*, 87.
14. Prolongo, S. G.; Moriche, R.; Jiménez-Suárez, A.; Sánchez, M.; Ureña, A. *Eur. Polym. J.* **2014**, *61*, 206.
15. Georgakilas, V.; Otyepka, M.; Bourlinos, A. B.; Chandra, V.; Kim, N.; Kemp, K. C.; Hobza, P.; Zboril, R.; Kim, K. S. *Chem. Rev.* **2012**, *112*, 6156.
16. Kim, N. H.; Kuila, T.; Lee, J. H. *J. Mater. Chem. A* **2013**, *1*, 1349.
17. Ryu, S. H.; Sin, J. H.; Shanmugharaj, A. M. *Eur. Polym. J.* **2014**, *52*, 88.
18. Lu, Y.; Zhang, F.; Zhang, T.; Leng, K.; Zhang, L.; Yang, X.; Ma, Y.; Huang, Y.; Zhang, M.; Chen, Y. *Carbon* **2013**, *63*, 508.
19. Liu, S.; Yu, B.; Zhang, T. *J. Mater. Chem. A* **2013**, *1*, 13314.
20. Hu, N.; Wang, Y.; Chai, J.; Gao, R.; Yang, Z.; Kong, E. S.-W.; Zhang, Y. *Sens. Actuators B* **2012**, *163*, 107.
21. Ramanathan, T.; Fisher, F. T.; Ruoff, R. S.; Brinson, L. C. *Chem. Mater.* **2005**, *17*, 1290.
22. Li, M.; Liu, C.; Cao, H.; Pan, J.; Zhao, H.; Zhang, Y. *Mater. Chem. Phys.* **2015**, *152*, 77.
23. Dreyer, D. R.; Park, S.; Bielawski, C. W.; Ruoff, R. S. *Chem. Soc. Rev.* **2010**, *39*, 228.
24. Huang, M.-R.; Peng, Q.-Y.; Li, X.-G. *Chem.–Eur. J.* **2006**, *12*, 4341.
25. Wang, Y.; Shi, Z.; Yin, J. *Polymer* **2011**, *52*, 3661.
26. Li, T.; Yuan, C.; Zhao, Y.; Chen, Q.; Wei, M.; Wang, Y. *High Perform. Polym.* **2013**, *25*, 348.
27. Jaidev, J.; Ramaprabhu, S. *J. Mater. Chem.* **2012**, *22*, 18775.
28. Li, X. G.; Huang, M. R.; Yang, Y. *Polymer* **2001**, *42*, 4099.
29. Li, X.-G.; Huang, M.-R.; Chen, R.-F.; Jin, Y.; Yang, Y.-L. *J. Appl. Polym. Sci.* **2001**, *81*, 3107.
30. Cao, Y.; Choi, H. J.; Zhang, W. L.; Wang, B.; Hao, C.; Liu, J. *Compos. Sci. Technol.* **2016**, *122*, 36.
31. Pham, Q. L.; Haldorai, Y.; Nguyen, V. H.; Tuma, D.; Shim, J.-J. *Bull. Mater. Sci.* **2011**, *34*, 37.
32. Dimiev, A. M.; Alemany, L. B.; Tour, J. M. *ACS Nano* **2013**, *7*, 576.
33. Suk, J. W.; Piner, R. D.; An, J.; Ruoff, R. S. *ACS Nano* **2010**, *4*, 6557.
34. Liu, H.-Y.; Wang, G.-T.; Mai, Y.-W.; Zeng, Y. *Compos. B* **2011**, *42*, 2170.
35. Balakrishnan, S.; Start, P. R.; Raghavan, D.; Hudson, S. D. *Polymer* **2005**, *46*, 11255.
36. Wang, X.; Jin, J.; Song, M. *Carbon* **2013**, *65*, 324.
37. Zaman, I.; Phan, T. T.; Kuan, H.-C.; Meng, Q.; Bao La, L. T.; Luong, L.; Youssf, O.; Ma, J. *Polymer* **2011**, *52*, 1603.